CO_2 abatement by two-dimensional MXene carbides†

Ángel Morales-García, Adrián Fernández-Fernández, Francesc Viñes* and Francesc Illas

Two-dimensional transition metal carbides with M_2C formula (M = Ti, Zr, Hf, V, Nb, Ta, Cr, Mo, W) have been recently synthesized and isolated, and are here presented as very promising candidates for carbon dioxide (CO_2) capture, storage, and activation. By means of density functional theory investigations including dispersion we show the strong CO_2 uptake and activation on M_2C, where estimates of adsorption and desorption rates indicate their CO_2 adsorption capacity even at low CO_2 partial pressures and high temperatures. The M_2C feature noteworthy CO_2 load capacities ranging 2.34–8.25 mol CO_2/kg, making them practical materials for CO_2 abatement.

The evergrowing carbon dioxide (CO_2) concentration in atmosphere is one of the major responsibles of the greenhouse effect, global warming, and ocean acidification.[1] This increase is ascribed mainly to anthropogenic activities connected to the combustion of fossil fuels, which nowadays demand alternative routes to reduce the CO_2 emissions.[2] There exist three primary approaches for reducing the amount of CO_2 in the atmosphere; (*i*) by acquiring energy efficient and conservation practices[3] which promote the dropping of CO_2 emissions; (*ii*) by reducing the carbon-based energy resources[4] using sustainable technologies such as hydrogen, solar and wind powers, and/or geothermal or biomass derived energies; and (*iii*) by CO_2 chemical trapping on active solid-substrates following the carbon capture and storage (CCS) derived strategy.[5]

Among these approaches, CCS appears to have a great potential[6-8] and has gained momentum since it is a feasible route to activate and then convert CO_2 into valuable chemical products, *e.g.* liquid fuels,[9] under ambient conditions. Here a solid-substrate is required to fix CO_2 but, ideally, one would choose one that activates it through charge transfer leading to a bent anionic $CO_2^{\delta-}$ species.[10,11] Such so-called activated CO_2 adsorbate is more prone to react when combined with other surface chemicals, *e.g.* H_2 for methanol production.[12] This waste-to-product route then not only reduces the CO_2 atmospheric content, but generates at the end of the chemical catalytic chain a saleable added-value product.

Several materials have been pointed for CO_2 capture/activation including metals,[13] metal oxides,[14] graphene-based materials,[15] zeolites,[16] and metal-organic frameworks (MOFs),[17] to name a few. Transition metal carbides (TMCs)[18] have recently raised much attention as a potential family of materials for CO_2 capture, storage, and activation,[19] with side appealing features including low-cost, thermal and physical robustness, and chemical stability.[20] The initial computational investigations were afterwards experimentally confirmed by CO_2 conversion at moderate temperatures.[21] Indeed, TMCs CO_2 capture and activation is predicted up to elevated temperatures and low CO_2 partial pressures.[19]

However, one technologically drawback of TMCs is their modest effectively exposed surface area ranging 20-450 m^2 g^{-1}.[22] More attractive are the TMCs two-dimensional (2D) derived counterparts, so-called MXenes —M and X stand for an early transition metal and carbon or nitrogen, respectively. More than 25 different MXene 2D materials have been synthesized from precursor MAX phases using hidrogen fluorine,[23] with at least three different stoichiometries: M_2X, M_3X_2, and M_4X_3,[24] although fluorine-free synthetic procedures have been recently implemented.[25] These 2D TMC display high surface areas in the order of 250-1000 m^2/g, conductivities comparable to multilayer graphene, and excellent stabilities.[23]

MXenes have been sucessfully used as alkaline-ion based batteries,[26,27] and catalysts for H_2 evolution from water.[28] As stated above, motivated by previous results on TMCs (001) surfaces[19] and by the MXenes large surface area, we investigated here the carbide MXenes capabilities for CO_2 sequestration. To facilitate a logical comparison to previous results and to circumvent structural-related effects, we restrained our study to d^2 (Ti, Zr, Hf), d^3 (V, Nb, Ta), and d^4 (Cr, Mo, W) MXenes having a 2:1 M:C ratio, exploring interaction through their (0001) exposed surface. Note that the (0001) surface is equivalent to the (111) surface of bulk refractory TMCs materials featuring face-centered cubic (fcc) crystallographic structure and 1:1 M:C ratio, a surface known to be less stable than (001).[29] Therefore, MXene materials allow one easier access to investigate such surfaces, which are thermodynamically disfavoured in their three-dimensional (3D) TMCs counterparts.[19]

The interaction of CO_2 with MXenes (0001) surfaces is here tackled by means of first-principles density functioal theory (DFT) based calculations within the generalized gradient approximation (GGA) using the Perdew-Burke-Ernzerhof (PBE) exchange-correlation functional,[30] as implemented in the Vienna *ab initio* simulation package (VASP).[31] Calculations have been carried out also including the D3 dispersion correction (PBE-D3) developed by Grimme.[32] In the following PBE-D3 zero-point energy (ZPE) corrected adsorption energies are discussed. Further computational details are given in the ESI.† For the sake of oncoming clarity, note that favourable adsorption energies, E_{ads}, are defined negative, and the more favourable interactions feature lower E_{ads} values.

To explore the CO_2 interaction with the selected MXenes, several adsorption sites have been evaluated implicitly considering different CO_2 molecular orientations with respect the material´s surface. After relaxation, five particular sites and/or conformations were identified as stable minima in at least one of the explored MXenes. These are labeled following the coordination notation as η^3-CO_2-μ^5-$C_CO_MO_M$, η^2-CO_2-μ^3-C_CO_B, η^3-CO_2-μ^5-$C_MO_CO_C$, η^2-CO_2-μ^3-C_MO_B, and η^1-CO_2-μ^2-C_B, and depicted in Fig. 1, where latter identification part is sufficient for its recognition —further details about notation are found in ESI†. Note that these sites are not always systematically found for all the explored MXene materials, and depend on each MXene (0001) surface (see ESI†). For instance, the C_CO_B site is generally the least favourable conformation and only competitive in Mo_2C, see Table 1; however $C_CO_MO_M$ is the most favourable site to adsorb CO_2 on several MXenes: Ti_2C, Zr_2C, Hf_2C, V_2C, Nb_2C, and W_2C. Neglecting dispersion terms raises the average E_{ads} by ~0.40 eV in (see Table S1 in ESI†) with no significant structural variations, in accord to previous studies on TMCs (001) surfaces.[19] Note in passing by that the obtained conformational minima are similar to those previously found on structurally resembling β-Mo_2C (0001) surface[32] and M_3C_2 MXenes,[34] although binding differences appear to occur as a function of the M:C ratio.

Further inspection of Table 1 shows remarkably high E_{ads}, ranging from -1.13 (W_2C) to -3.69 eV (Ti_2C). So, carbide M_2C MXenes essentially double the CO_2 bond strength compared equivalent values on parent TMC (001) surfaces, ranging from -0.70 (NbC) to -1.65 (HfC) eV.[19] Furthermore, values spread, including the non-CO_2 attaching case of Cr_2C. Table 1 data shows an E_{ads} decrease (weaker adsorption) when moving along a *d* series, in agreement with the observed CO_2 adsorption on TMCs and M_3C_2 MXenes.[19,34] Note that, despite this high energy attachment, CO_2 molecules remain intact yet bent —angles α(OCO) in the 113-135° range, with elongated C-O bonds —distances δ(CO) in the 1.26-1.51 Å interval, see further details in Table S1 of ESI†. At this stage, the high adsorption energies and structural data support MXenes utilization in CO_2 capture and activation, evidented by a high charge transfer according to Bader atoms-in-molecules analysis[35] which confirms the formation of highly anionic $CO_2^{\delta-}$ species with δ- Bader values between -0.90 and -2.86 *e*. The unprecendented high-negative adsorbed CO_2 species on Hf_2C, with δ- above -2 *e*, seems to imply a higher activity, pointing this MXene for CO_2 conversion purposes.

Table 1 Adsorption energies of CO_2 on stable sites of carbide MXenes (0001) surfaces as obtained at PBE-D3 level, ZPE-corrected. PBE and further details are given in Table S1 of the ESI.† All values are given in eV.

		$C_CO_MO_M$	C_B	$C_MO_CO_C$	C_MO_B	C_CO_B
d^2	**Ti_2C**	-3.69	—	-3.47	—	-2.88
	Zr_2C	-3.16	—	-3.03	—	—
	Hf_2C	-3.36	—	-3.33	—	—
d^3	**V_2C**	-2.41	-2.05	-2.36	-2.31	—
	Nb_2C	-2.03	-1.99	-2.01	-2.11	—
	Ta_2C	—	-1.87	-2.37	-2.37	—
d^4	**Cr_2C**	—	+0.63	—	—	—
	Mo_2C	—	-1.61	—	-1.63	-1.47
	W_2C	-1.31	-1.13	—	—	—

Due to the noteworthy CO_2 attachment and activation on carbide MXene (0001) surfaces, it is worth investigating the range of temperatures at which the MXenes would capture and store CO_2. To this end, transition state theory (TST)[36] based methodology is used to estimate adsorption and desorption rates (r_{ads} and r_{des}) over a temperature range up to 2500 K, well below the melting points of parent TMCs, ranging 2900-4200 K.[37] Details on TST models are found in ESI.† Briefly, the adsorption rate depends on the incidence of CO_2 to the surface and so on the CO_2 partial pressure (p_{CO2}). Three different p_{CO2} conditions are evaluated to calculate r_{ads}: (*i*) atmospheric CO_2 partial pressure, p_{CO2} = 40 Pa,[38] (*ii*) for p_{CO2} = 15000 Pa (or 0.15 bar),[39] a benchmark value for postcombustion exhaust gases, and (*iii*) $p_{CO2} = 10^5$ Pa (or 1 bar), a partial pressure regime of interest for pure CO_2 stream generation from a CCS system.[40]

The desorption rates largely depend on the adsorption strenght, and this depends as well on the adsorption conformation (see Table 1). Two desorption fringe situations are considered gaining two temperature-dependent desorption curves for each MXene, either using the weakest E_{ads} value as obtained by PBE and the strongest E_{ads} as obtained by PBE-D3. This choice comprises the least and most favourable adsorption situations, without being biased by the computational accuracy. The estimated r_{ads} and r_{des} are illustrated for extreme situations of W_2C and Ti_2C, with lowest and highest E_{ads} values, respectively (see Fig. 2a, Table 1 and Table S1 in ESI†).

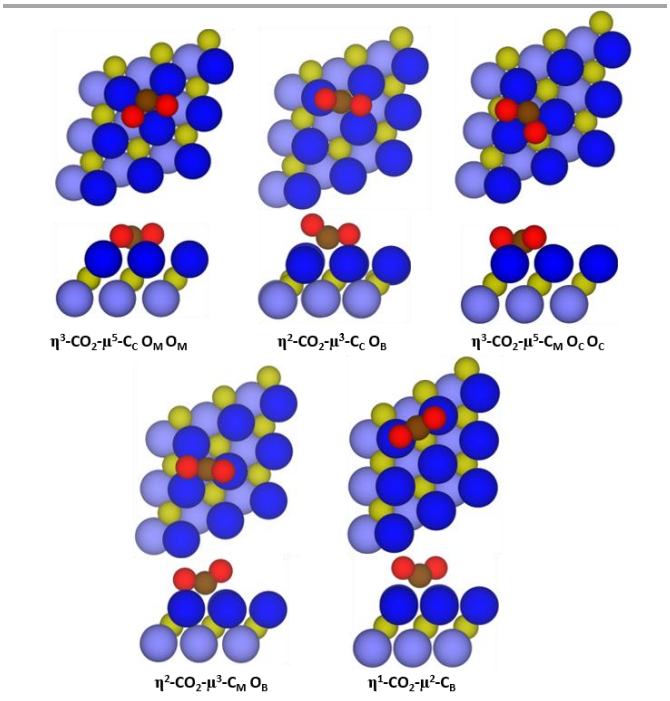

Fig.1 Side and top views of CO_2 adsorbed on η^3-CO_2-μ^5-$C_CO_MO_M$, η^2-CO_2-μ^3-C_CO_B, η^3-CO_2-μ^5-$C_MO_CO_C$, η^2-CO_2-μ^3-C_MO_B, and η^1-CO_2-μ^2-C_B sites of MXene (0001) surfaces. Carbon and oxygen atoms of the CO_2 molecule are represented by brown and red spheres, respectively. MXene (0001) surface is defined with dark and light blue spheres for M upper and bottom layers, respectively, whereas inner carbon layer is represented by dark yellow spheres. Further structural details are found in ESI.†

In Fig. 2a that crossing points between r_{ads} and r_{des} define temperatures below which adsorption prevails and, consequently, CO_2 becomes stored. Thus, for W_2C at 40 Pa p_{CO2} (labeled air), the intersection temperature T_1 is 344 K for weakest PBE E_{ads}, and 696 K (T_2) for strongest PBE-D3 E_{ads}. T_1-T_2 defines a temperature range below which CO_2 would certainly be stored, and above which it would be certainly desorbed. Note that an increase of p_{CO2} to $15{\cdot}10^3$ Pa shifts these limits T_3-T_4 to higher, even further at 1 bar pressure in the T_5-T_6 limit. These three intervals imply temperature ranges where the initial capture and accumulation of CO_2 is lost when the system is annealed. The average swich temperature for the set of MXene surfaces is ~ 1250 K (see Fig. 2b), well below that the melting points of parent TMCs, ranging 2900-4200.[37]

Considering this interpretation, the analysis of the rest of MXenes is summarized in Fig. 2b. Note that here only temperature ranges are shown, independent of the particular adsorption site and strength; a further detailed description is reported in Table S2 of the ESI.† From Fig. 2b one notices that consistently those MXene (0001) surfaces with high adsorption energies feature elevated temperature ranges. Therefore, d^2 MXenes (Ti_2C, Zr_2C, Hf_2C) show the largest temperature ranges, whereas d^4 MXenes feature the smallest. Notice in passing by that Cr_2C was excluded from rate analysis as features (unfavourable) positive E_{ads}, see Table 1. For practical purposes, Mo_2C and W_2C are among the most appealing MXenes in case of CO_2 capture and posterior release processes.

Last, surface exposure and possible CO_2 loading is considered. One main appealing feature of 2D MXene materials is their high surface area. Considering our models dimensions (see ESI†), four molecules of CO_2 could be conserbvatively and simultaneously adsorbed on each MXene material surface. For such an idealized situation, one could quantify the amount of CO_2 adsorbed per amount of MXene. Present estimations indicate that carbide MXenes can adsorb 2.34–8.25 mol CO_2/kg. of substrate, see Fig. 3 and Table S3 of the ESI†. This range clearly shows the high potential of MXene materials for CO_2 storage being comparable or even better than zeolites, *e.g.* Ca-X[41] and I3X[42] with 3.36 and 3.96 mol CO_2/kg, respectively, or derivates of graphene, *e.g.* a-RGO-950[43] with 3.36 mol CO_2/kg, which are clearly better than using bulk MgO nanopowders, with 0.92 mol CO_2/kg.[44] In practical operation conditions one should separate CO_2 from other competing (combustion) gases prior to adsorption, although recent studies on a series of Mxenes show a high adsoprtion preference for CO_2 with respect other gases such as CO or CH_4 by more than 1.5 eV.[45]

In summary, CO_2 storage on carbide M_2C MXenes (M = Ti, Zr, Hf, V, Nb, Ta, Mo, W) (0001) surfaces is reported by using the state-of-art DFT PBE calculations including D3 Grimme correction dispersion. Results show high adsorption energies up to -3.69 eV accompanied by a CO_2 activation, translated into anionic $CO_2^{\delta-}$ species with elongated δ(CO) bonds, bent structures, and a MXene→CO_2 charge transfer, unprecedentedly above 2 *e* for Hf_2C. Given these high adsorption energies, M_2C MXenes are predicted to be more effective than their 3D bulk counterparts for CO_2 capture, storage and activation. Adsorption and desorption rates predicted

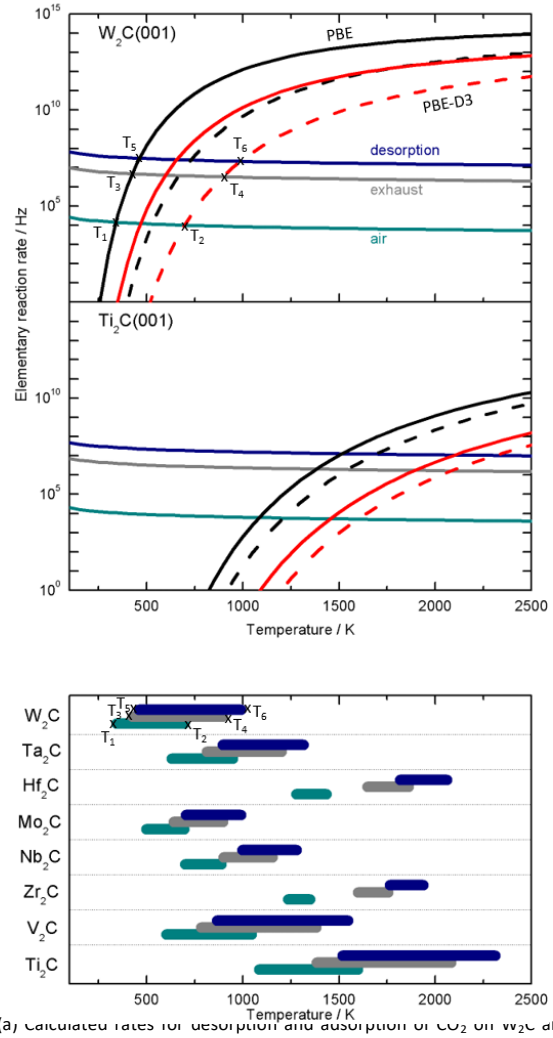

Fig. 2 (a) Calculated rates for desorption and adsorption of CO_2 on W_2C and Ti_2C (0001) surfaces. On W_2C marked points with T_1–T_6 labels in (a) and (b) show how desorption temperature ranges in (b) have been obtained. Legend for (a): green, gray, and blue colors correspond to adsorption rates on a single site per time unit for a CO_2 partial pressures of 40, $15{\cdot}10^3$, and 10^5 Pa, respectively. Black and red lines are desorption rates per site for PBE (solid) and PBE-D3 (dashed). Legend for (b): green, gray, and blue bars belong to desorption temperatures ranges for CO_2 partial pressures of 40, $15{\cdot}10^3$, and 10^5 Pa, respectively.

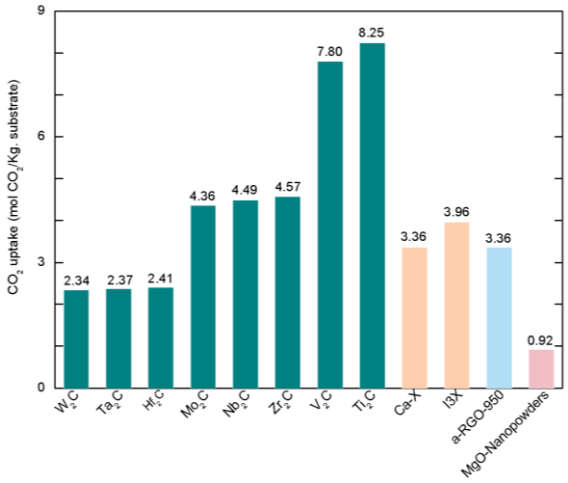

Fig. 3 Comparison of CO_2 uptake in MXene materials with zeolites (Ca-X and I3X), derivates of graphene (a-RGO-950) and bulk MgO nanopowders depicted by green, orange, blue and pink bars, respectively. Further details are found in Table S3 of the ESI.†

from TST models show that these materials can theoretically adsorb CO_2 up to elevated temperatures and low partial pressures. Additionally, MXenes can yield CO_2 uptakes ranging 2.34–8.25 mol CO_2/kg of substrate, quite competitive to other nowadays-existent material solutions. Thus, 2D carbide M_2C MXenes are introduced as potential materials for CO_2 capture, where its activated adsorption is further appealing for using them as catalysts on CO_2 conversion.

This work has been funded by Spanish *Ministerio de Economía y Competitividad* (MEC) CTQ2015-64618-R grant, partly by *Generalitat de Catalunya* grants 2014SGR97 and XRQTC, and the NOMAD Center of Excellence project, which received funding from the European Union's Horizon 2020 research and innovation programme under Grant Agreement No. 676580. A. M. G. and F. V. thank the Spanish *Ministerio de Economía y Competitividad* for the *Juan de la Cierva* (FJCI-2015-23760) and the *Ramón y Cajal* (RYC-2012-10129) postdoctoral grants, respectively. F. I. acknowledges additional support from the 2015 ICREA Academia Award for Excellence in University Research.

Notes and references

1 Intergovernmental Panel on Climate Change, *Climate Change 2014*: *Synthesis Report*. IPCC, 1st edn, 2015.

2 V. Balzani, A. Credi and M. Venturi, *ChemSusChem*, 2008, **1**, 26.

3 J. O. Lewis, S. N. Hógáin and A. Borghi, *Building Energy Efficiency in European Cities*. 2013.

4 P. A. Owusu and S. Asumadu-Sarkodie, *Cogent Engineering*, 2016, **3**, 1167990.

5 D. Y. C. Leung, G. Caramanna and M. M. Maroto-Valer, *Renew. Sust. Energ. Rev.*, 2014, **39**, 426.

6 K. P. Kuhl, E. R. Cave, D. N. Abram and T. F. Jamarillo, *Energ. Environ. Sci.*, 2012, **5**, 7050.

7 C. W. Li and M. W. Kanan, *J. Am. Chem. Soc.*, 2012, **134**, 7231.

8 M. Favaro, H. Xiao, T. Cheng, W. A. Goddard III, J. Yano and E. J. Crumlin, *Proc. Natl. Acad. Sci. USA*, 2017, **114**, 6706.

9 J. Wei, Q. Ge, R. Yao, Z. Wen, C. Fang, L. Guo, H. Xu and J. Sun, *Nat. Commun.*, 2017, **8**, 15174.

10 F. Viñes, A. Borodin, O. Höfft, V. Kempter and F. Illas, *Phys. Chem. Chem. Phys.*, 2005, **7**, 3866.

1 1 H. J. Freund and M. W. Roberts, *Surf. Sci. Rep.*, 1996, **25**, 225.

12 S. Posada-Pérez, P. J. Ramírez, J. Evans, F. Viñes, P. Liu, F. Illas and J. A. Rodríguez, *J. Am. Chem. Soc.*, 2016, **138**, 8269.

13 V. A. de la Peña O´Shea, S. González, F. Illas and J. L. G. Fierro, *Chem. Phys. Lett.*, 2008, **454**, 262.

14 D. C. Sorescu, J. Lee, W. A. Al-Saidi and K. D. Jordan, *J. Chem. Phys.*, 2005, **109**, 104707.

15 Y. Jiao, A. Du, Z. Zhu, V. Rudolph, G. Q. Lu and S. C. Smith, *Catal. Today*, 2011, **175**, 271.

16 D. Smykowski, B. Szyja and J. Szczygiel, *J. Mol. Graphics Modell.*, 2013, **41**, 89.

17 C. A. Trickett, A. Helal, B. A. Al-Maythalony, Z. H. Yamani, K. E. Cordova and O. M. Yaghi, *Nat. Rev. Mater.*,2017, **2**, 17045.

18 Y. Xiao, J.-Y. Hwang and Y.-K. Sun, *J. Mater. Chem. A*, 2016, **4**, 10379.

19 C. Kunkel, F. Viñes and F. Illas, *Energy Environ. Sci.*, 2016, **9**, 141.

20 F. Viñes, C. Sousa, P. Liu, J. A. Rodriguez and F. Illas, *J. Chem. Phys.*, 2005, 122, 174709.

21 X. Liu, C. Kunkel, P. Ramírez de la Piscina, N. Homs, F. Viñes, and F. Illas, *ACS Catal.*, 2017, **7**, 4323.

22 C. Giordano, C. Erpen, W. Yao, B. Milke and M. Antonietti, *Chem. Mater.*, 2009, **32**, 5136.

23 M. Naguib, O. Mashtalir, J. Carle, V. Presser, J. Lu, L. Hultman, Y. Gogotsi and M. W. Barsoum, *ACS Nano*, 2012, **6**, 1322.

24 B. Anasori, M. R. Lukatskaya and Y. Gogotsi, *Nat. Rev. Mater.*, 2017, **2**, 16098.

25 X. Yu, X. Cai, H. Cui, S.-W. Lee, X.-F. Yu, B. Liu, *Nanoscale*, 2017, **9**, 17859.

26 Y. Xie, M. Naguib, V. N. Mochalin, M. W. Barsoum, Y. Gogotsi, X. Yu, K. W. Nam, X. Q. Yang, A. I. Kolesnikov and P. R. C. Kent, *J. Am. Chem. Soc.*, 2014, **136**, 6385.

27 D. Er, J. Li, M. Naguib, Y. Gogotsi and V. B. Shenoy, *ACS Appl. Mater. Interfaces*, 2014, **6**, 11173.

28 W. F. Chen, C. H. Wang, K. Sasaki, N. Marinkovis, W. Xu, J. T. Muckerman, T. Zhu and R. R. Adzic, *Energy Environ. Sci.*, 2013, **6**, 943.

29 A. Vojvodic, C. Ruberto and B. I. Lundqvist, *J. Phys.: Condens. Matter*, 2010, **22**, 375504.

30 J. P. Perdew, K. Burke and M. Ernzerhof, *Phys. Rev. Lett.*, 1996, **77**, 3865.

31 G. Kresse and J. Furthmüller, *Phys. Rev. B: Condens. Matter Mater. Phys.*, 1996, **54**, 11169.

32 S. Grimme, S. Ehrlich and L. Goerigk, *J. Comput. Chem.*, 2011, **32**, 1456.

33 S. Posada-Pérez, F. Viñes, P. J. Ramírez, A. B. Vidal, J. A. Rodriguez and F. Illas, *Phys. Chem. Chem. Phys.*, 2014, **16**, 14912.

34 L. M. Azofra, N. Li, D. R. MacFarlane and C. Sun, *Energy Environ. Sci.*, 2016, **9**, 2545.

35 R. F. W. Bader, *Acc. Chem. Res.*, 1985, **18**, 9.

36 K. Reuter, in *Modelling and Simulation of Heterogeneous Catalytic Reactions*, Wiley-VCH Verlag GmbH & Co. KGaA, 2011, ch. 3.

37 L. E. Toth, *Transition Metal Carbides and Nitrides*, Academic Press: New York, 1971.

38 T. Takahashi, S. Sutherland and A. Kozyr, *Global Ocean Surface Water Partial Pressure of CO_2 Database: Measurements Performed During 1957-2014 (Version 2014)*, Environmental Sciences Division. Oak Ridge National Laboratory, 2015.

39 D. M. D´Alessandro, B. Smit and J. R. Long, *Angew. Chem. Int. Ed.*, 2010, **49**, 6058.

40 M. E. Boot-Handford, J. C. Abanades, E. J. Anthony, M. J. Blunt, S. Brandani, N. Mac Dowell, J. R. Fernández, M.-C. Ferrari, R. Gross, J. P. Hallett, R. S. Hazseldine, P. Heptostall, A. Lyngfelt, Z. Makuch, E. Mangano, R. T. J. Porter, M. Pourkashanian, G. T. Rochelle, N. Shah, J. G. Yao and P. S. Fennell, *Energy Environ. Sci.*, 2014, **7**, 130.

41 T.-H. Bae, M. R. Hudson, J. A. Mason, W. L. Queen, J. J. Dutton, K. Sumida, K. J. Micklash, S. S. Kaye, C. M. Brown and J. R. Long, *Energy Environ. Sci.*, 2013, **6**, 128.

42 C. Chen, D.-W. Park and W.-S. Ahn, *Appl. Surf. Sci.*, 2014, **292**, 63.

43 S. Chowdhury and R. Balasubramanian, *Ind. Eng. Chem. Res.*, 2016, **55**, 7906.

44 W. Gao, T. Zhou, B. Louis, Q. Wang, *Catalysts* 2017, **7**, 116.

45 N.Li, X. Chen, W.-J. Ong, D. R. MacFarlane, X. Zhao, A. K. Cheetham, C. Sun, *ACS Nano* 2017, **11**, 10825.